Arabian Journal for Science and Engineering (2023) 48:14059–14078
https://doi.org/10.1007/s13369-023-08052-9

RESEARCH ARTICLE-CIVIL ENGINEERING

Improvement of an Undisturbed Peat Soil with Jet Grout Columns: Physical and Numerical Modeling

Hakan Yalcin[1] · Zulkuf Kaya[2] · Cenk Cuma Çadir[3] · Erdal Uncuoğlu[2] · Aykut Erol[2] · Muge Akin[1]

Received: 16 November 2022 / Accepted: 13 June 2023 / Published online: 6 July 2023

Abstract
The bearing capacity of the composite-formed soil, such as grouted peat soil, is a crucial design parameter that can be improved by employing jet grout columns (JGCs). The coupling effect of the requirement of new industrial sites and reduction in the suitable regions for construction requires research on improving the bearing capacity of abundantly available peat soils. Despite routinely reported studies on peat soil, improvement studies basically took upon the disturbed soil samples. Research on the sample collecting techniques or experiments on undisturbed peat soil has not been conducted intensively. This study uses a domestic jet grout device to compare features of the undisturbed peat soils at the laboratory using axial loading tests. While samples were collected undisturbedly using specially designed steel boxes, the peat soil within the steel boxes was improved by jet grout columns. Additionally, PLAXIS 3D simulations were used to estimate the behavior of the improved soil. Results showed that the bearing capacity of the soil increased 4 times for square foundations (2 × 2 JGC) and 4.5 times for strip foundations (3 × 1 JGC) compared to the unimproved organic soil.

Keywords Peat soils · Jet grout columns · Improvement · Physical and numerical modeling

1 Introduction

The organic soils (OS) are often challenging to use for construction purposes (residential buildings, industries, and other infrastructure facilities) by engineers, for having low shear strength and high compressibility features [1, 2]. The rapid development of developing countries caused the construction of production facilities and industrial areas to fetch the needs of society. This situation also caused the secrecy of the reliable sites. Currently, alternate sites must be considered even if they have poor engineering performance by developing modern engineering methods to improve their deficiencies. For example, one of the densely industrialized zone in Kayseri (KFZ) has a peatland of approximately 2400 ha. As for the international perspective, peat soils cover 4 million km^2 in over 500 different regions [3–5].

OS is regarded as soft or weak soil, and buildings constructed on such soils are exposed to various engineering challenges. It is essential to determine soil behavior correctly to overcome the challenges, such as bearing capacity problems, high deformation, and settlement issues. Since extensive research dealing with soft soil improvement has only been carried out in the laboratory environment on the disturbed soil, merely relying on such studies is not engineeringly feasible. Research on undisturbed soil is inevitable for an accurate estimate of soft soil behavior. Undisturbed block sampling provides reliable data for calculation of the settlement and bearing capacity of OS [6–8].

✉ Zulkuf Kaya
zkaya@erciyes.edu.tr

Hakan Yalcin
hakan.yalcin@agu.edu.tr

Cenk Cuma Çadir
cenk.cadir@bozok.edu.tr

Erdal Uncuoğlu
erdalu@erciyes.edu.tr

Aykut Erol
aykuterol@erciyes.edu.tr

Muge Akin
muge.akin@agu.edu.tr

[1] Department of Civil Engineering, Abdullah Gül University, Kayseri, Turkey

[2] Department of Civil Engineering, Erciyes University, Kayseri, Turkey

[3] Department of Civil Engineering, Yozgat Bozok University, Yozgat, Turkey

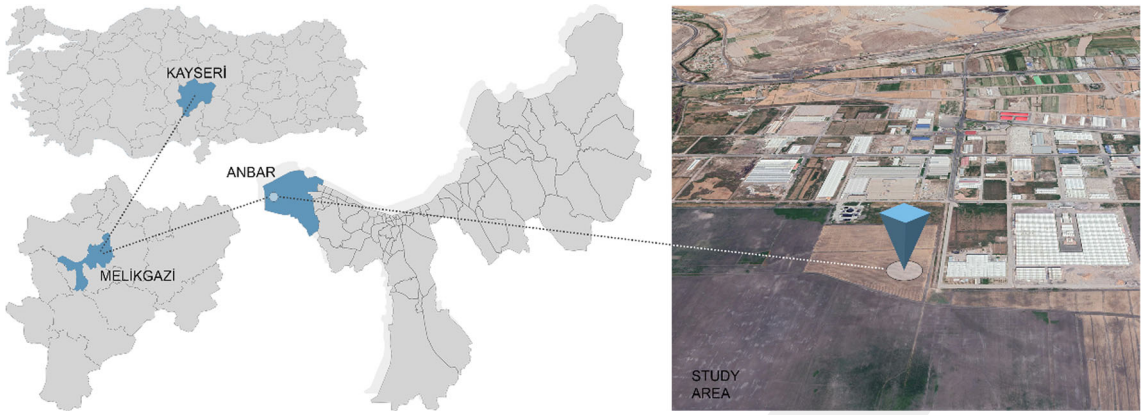

Fig. 1 Location map of the study site

However, collecting the samples undisturbedly is a challenging job, and strains induced on samples during the collection process, swelling, stress relief, and changes in moisture content during storage are some mechanisms by which disturbances might be introduced [9, 10]. Efforts must be made either by improving the sample collecting techniques or by employing appropriate apparatus to collect the samples undisturbedly. The block sampling method incorporated in this project is an attempt to solve this issue.

As for improving the bearing capacity of soft soils, jet grouting systems are industrially active and considerably useful, practical, and efficient. This is because the bearing capacity of the soft soil increases by transferring loads onto the grout columns. As for the installation of the grout columns, jet grouting is constructed using the injection of lime or cement under pressure into the soil. The dimensions and shape of the jet grout columns (JGCs) can be affected by jet pressure, rotation, and lifting speed [11].

Many recent studies have dealt with load-carrying capacities and settlements of grouted soft soil conducted and modeled using the finite element method by several researchers [12–14]. The construction of many jet-grouted columns in general creates a challenge that is difficult to analyze, and numerical methods are increasingly used to estimate the performance of improved soil.

This multi-aspect study aims to highlight the positive impact of JGCs on the bearing capacity and settlement behavior of the undisturbed OS. While engineering efforts were made to collect the samples from the sites undisturbedly using specially designed steel boxes, the features of the soil were analyzed and compared with the site conditions. Steel boxes assisted in undisturbed sample collection and conduction of the loading tests. The dimensions of the steel boxes were determined according to the preliminary finite element (PLAXIS 3D) analysis.

A jet grouting device was designed to be compatible with the steel boxes and used for installing the JGCs into the OS. The dimensions of the grout columns were determined as a result of various optimization experiments. While 2 × 2 and 3 × 1 JGCs configurations of the columns within the soils were used, square and rectangular footing setups were used for loading tests. PLAXIS 3D was also performed to model improved soil behavior, and simulation results were compared with the actual experiments.

2 Physical Modeling

2.1 Site Characterization

This study involved three different materials: OS, silty sand, and cement. The undisturbed OS samples were collected from the Kayseri Free Zone (Fig. 1), KFZ, and an area of about 7 million square meters within the boundaries of the Kayseri Province of Turkey.

The standard penetration tests were performed at the research site to define the site characteristics of OS. The log of boreholes (BH-1, BH-2, and BH-3) is given in Fig. 2. The soil profile consisted of silty clay, OS, silty sand, and low plasticity clay from top to bottom. The OS was composed of plant roots, sedges, and fibers.

Figure 2 shows silty clay and topsoil combinations from the surface between 0.3 and 0.5 m. Below this layer, there are OS deposits that contain clay bands that range from 50 to 200 mm in thickness. The top of the OS deposit (between the surface and a depth of about 1.0–1.6 m) contains sedges, plant roots, coarse fibers, and some silty clayey soil, whereas the lower levels consist of the finer fibrous and amorphous OS. Figure 3a shows the cut operation until the water table is reached and the steel test boxes are placed. The boxes were pushed into the peat to collect the undisturbed OS (Fig. 3b). The clay band, fibrous, amorphous peat, and fibers can be seen in Fig. 3c.

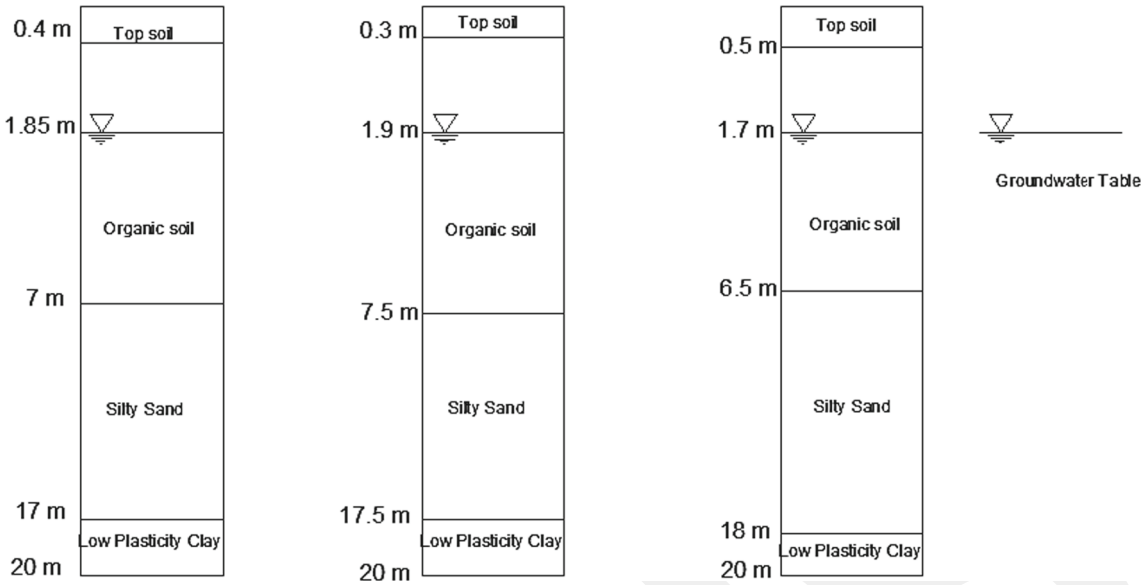

Fig. 2 Borehole logs of SPT from the site (BH-1, BH-2, BH-3)

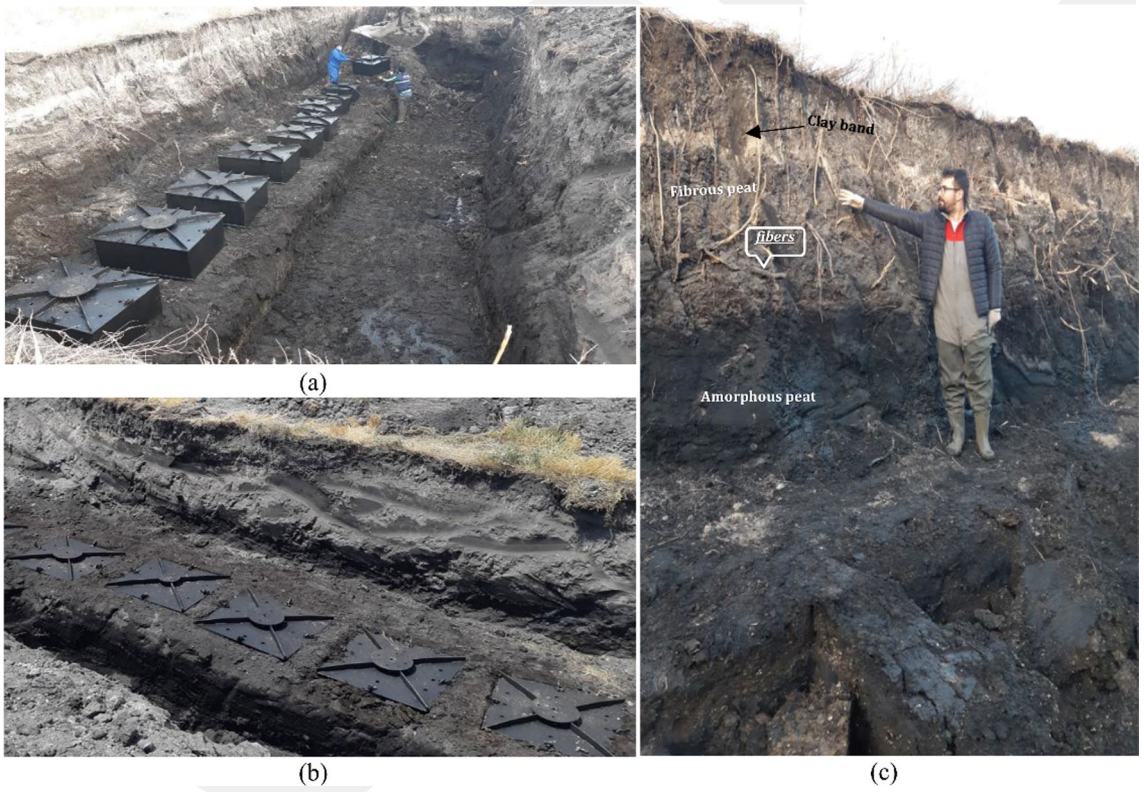

Fig. 3 **a** Cut operation until water table and placing the boxes, **b** pushing the boxes inside peat, **c** soil layers and fibers sampling of undisturbed organic soil

Fig. 4 **a** The schematic view of DCP, **b** performing DCP test on-site, **c** performing DCP test in the laboratory

Table 1 The recommended methods for evaluating the disturbance of samples (quality) [18]

Method	Parameter	Sample quality			
		Very good to excellent	Good to fair	Poor	Very poor
Andresen and Kolstad [19]	ε_v	< 1	1–4	4–10	> 10
Lunne et al. [16] for OCR = 1–2	$\Delta e/e_0$	< 0.04	0.04–0.07	0.07–0.14	> 0.14
Lunne et al. [16] for OCR = 2–4	$\Delta e/e_0$	< 0.03	0.03–0.05	0.05–0.10	> 0.10
Karlsrud and Hernandez-Martinez [20]	M_0/M_L	> 2	1.5–2.0	1.0–1.5	< 1

ε_v = Volume change, e_0 = Initial void ratio, OCR = Over-consolidation ratio, Δe = Change in void ratio, σ_{v0}' = Effective stress, M_0/M_L = Oedometer stiffness ratio

The degree of disturbance (i.e., quality) of block samples of the soft soils is critical.

In this research, the thickness of the boxes was 10 mm to provide the necessary rigidity against bending moments while pushing and lifting approximately 350 kg of peat soil. The thickness was chosen based on the results of computer-aided solid modeling software. In addition, the cutting edges of the sample boxes were designed and sharpened similarly to the thin-walled tube to provide easy penetration and collect undisturbed sampling. The degree of undisturbance of the sample collected by various methods can be expressed by the area ratio (A_r) for thin-walled tube sampling [15], which is given as follows:

$$A_r = \frac{D_o^2 - D_i^2}{D_i^2} \quad (1)$$

where D_i is the inner diameter of the cutting edge, D_o is the outer diameter of the cutting edge. A soil sample generally can be undisturbed if A_r is less than 10%. According to Eq. 1, the value of A_r for this research is calculated as 4.9%; peat samples can be accepted as undisturbed.

According to Lunne et al., the evaluation of the disturbance quality is based on the normalized void ratio ($\Delta e/e_0$) and over-consolidation ratio (OCR) [16]. Thus, consolidation tests were carried out in the current study following the procedures outlined in ASTM D2435 [17]. The quantification of sample disturbance is listed in Table 1.

The volumetric change rate (ε_v) was determined as 0.032–0.710. The normalized void ratio variation ($\Delta e/e_0$) and over-consolidation ratio (OCR) were 0.009–0.0254 and 1.55–1.90, respectively. The sample quality of the OS, taken as a block from the study site, was determined to be 'very good to excellent' as per Table 1.

A detailed explanation of sample quality for this soil type can be found in the reference [18]. In addition to the consolidation test, dynamic cone penetration (DCP) and vane shear test (VST) were performed to check the samples' disturbance level. DCP test measures the strength of in situ soil and the thickness of subsurface soil layers [21]. The test is carried out by repeatedly striking a metal cone with an 8 kg weight dropped from a distance of 575 mm. The schematic view of the device and DCP tests in the field and laboratory can be seen in Fig. 4.

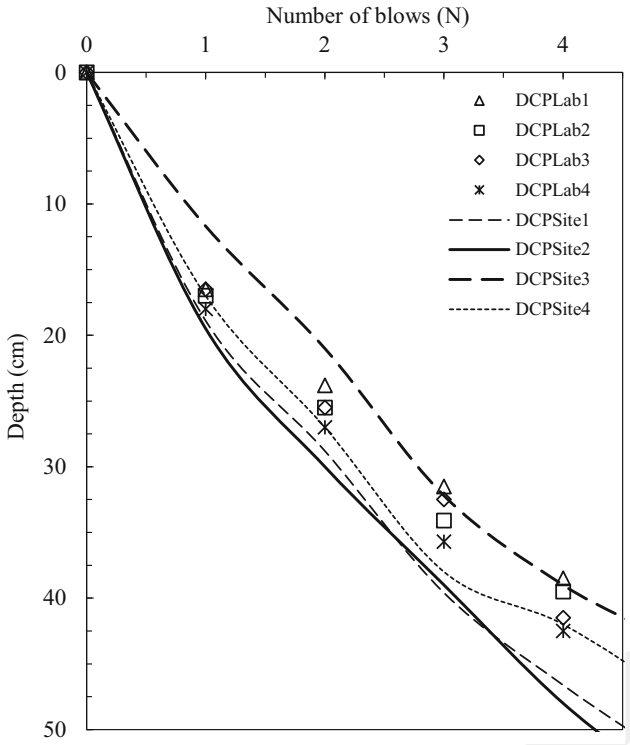

Fig. 5 The penetration curves of the DCP test for site and laboratory

DCP test was performed at the same depth as the samples were taken. In the site, penetration of as long as 500 mm was observed to compare the results obtained at the laboratory. The DCP tests could only penetrate until 400 mm in the laboratory as the penetration limit is restricted by the depth of the boxes (450 mm). However, despite the difference in the penetration lengths, the penetration curves of both types of experiments were similar, as shown in Fig. 5. Hence, it can be claimed that the samples were transported to the laboratory in good quality.

The VST determines the undrained shear strength of soils, especially for soft clays [22]. VST can be performed at both the laboratory and the site. The torque and c_u values obtained from the undrained shear strength tests are given in Table 2. It can be seen that the values for both locations are similar. From this point of view, it can be said that the amount of sample disturbance is relatively low, if it is present at all.

2.2 Material Properties

The particle size distribution curves obtained from the sieve analysis and hydrometer test for OS and sand are illustrated in Fig. 6 according to the ASTM D421-85 and ASTM D422-63 standards [23, 24].

The geotechnical properties of OS and silty sand are listed in Table 3. Unconfined compression tests, direct shear tests, permeability, and pH tests were performed at Erciyes University Soil Mechanics Laboratory. The moisture content of OS was determined as the mean value of three samples obtained at the site. The organic matter content of the OS samples was determined using a high-temperature furnace based on the ASTM D2974-00 standards [25]. The laboratory fall cone test determines soft soils' consistency limits (liquid and plastic limits). Results were more satisfactory than the Casagrande test because the groove opening was not appropriate due to the fibers of peats [26].

The soil strength parameters were obtained using a direct shear test. The undisturbed samples were sheared at a constant shear rate of 0.5 mm/min according to the ASTM D3080 standard [32]. Tests were conducted using a traditional oedometer test, where the time to failure was set as $t_{50}/8$ (t_{50} represents the time to 50% consolidation). 10, 20, and 40 kPa and 50, 100, and 150 kPa were chosen as two normal stress groups, which are also compatible with the research of Amuda et al. [31, 35]. The strength parameters were obtained as $c' = 9.7$ kPa and $\phi' = 29.8°$. Compared to soft soil, these strength parameters seem high, but according to Landva and La Rochelle, the internal friction angle of peat is often higher than inorganic soil. Den Haan et al. reported the internal friction angles as 32° to 58° for peat soils [36, 37].

Ulusay et al. investigated the geo-engineering characteristics of peat soils from the KFZ area and reported internal friction angles between 42.6° and 59.8° [38]. Since peat fibers are not constantly solid and can be periodically filled with water and gas, their high friction angle might not be solely influential in causing high shear strength. Due to the fibers' reinforcement effects, the fibers' existence changes how peat behaves in terms of shear strength [39, 40]. After the geotechnical parameters of OS were obtained, the direct shear test was performed for the sand layer. The sand specimen was compacted in the shear box with 60 mm width and 20 mm thickness at a relative density of 60%. Cohesion and internal friction angles for sand were 10.70 kPa and 41.2°, respectively.

X-ray fluorescence (XRF) analyses were performed to determine the components of the OS, as shown in Table 4. As a result of the analysis, the highest content of silicon oxide (SiO_2), calcium oxide (CaO), and aluminum oxide (Al_2O_3) was determined as 62.2%, 15.1%, and 10.8%, respectively.

The cement used for grout is Portland Cement (PC) type CEM I-42.5R, according to ASTM C150 [41]. All laboratory-scale jet grout columns were installed at a water-cement ratio of 1:1, and the grout density was 1.45 g/ml. The water/cement ratio was similar to that used on the site.

Table 2 Undrained shear strength test results of OS (site and laboratory)

Test No.	Site		Laboratory	
	Torque (kg cm)	c_u (kg/cm^2)	Torque (kg cm)	c_u (kg/cm^2)
1	338.6	0.188	336.6	0.178
2	489.6	0.262	496.2	0.268
3	469.2	0.250	479.1	0.255
4	487.5	0.261	520.2	0.277
5	417.1	0.223	459.0	0.244
6	392.7	0.209	387.6	0.206
7	342.7	0.183	357.0	0.190
8	405.9	0.216	418.2	0.223

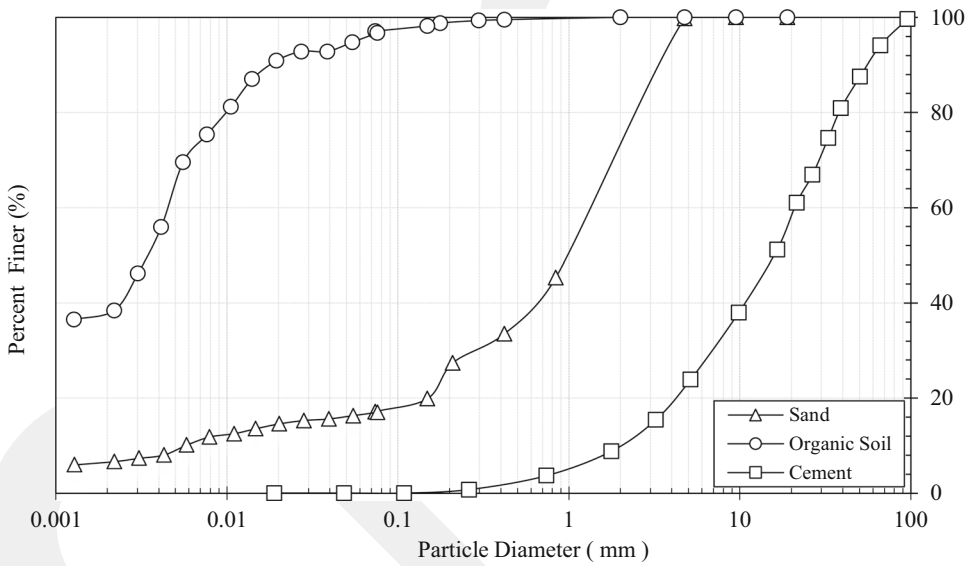

Fig. 6 Grain size distribution curves of soils and cement

Table 3 Physical properties of organic soil and silty sand

Material name	Organic soil	Silty sand
Moisture content (ω), % [27]	184.8	–
Specific gravity [28],	1.93	2.70
Liquid limit (LL), % [29]	221.5	–
Plastic limit (PL), % [29]	98.7	–
Plasticity index (PI), %	122.8	–
Unconfined compressive strength (q_u), kN/m^2 [30]	22.3	–
Undrained shear strength (c_u), kN/m^2 [31]	9.7	10.70
Internal friction angle (ϕ), degree [32]	29.8	41.20
Permeability coefficient, (k) m/day [30]	1.38×10^{-6}	0.86×10^{-3}
pH [33]	8.9	–
Unified soil classification system (USCS) [34]	High plasticity organic clay (OH)	Silty sand (SM)
Von post classification system	H4–H6	–
Ash content (AC), % [25]	High ash content (ash content % 34)	–

Table 4 Chemical and physical properties of organic soil and ordinary Portland cement

Composition	Organic soil (%)	Portland cement (%)
SiO_2	62.20	12.75
CaO	15.10	67.45
Al_2O_3	10.80	3.54
Fe_2O_3	3.70	7.32
MgO	3.90	1.27
Na_2O	1.50	0.39
K_2O	1.20	0.94
SO_3	0.16	4.86

2.3 Testing Equipment

The testing equipment consisted of sample collecting boxes, a jet grout system, a data logger, transducers, and footings. The steel boxes consisted of three parts: the main body, the top cover, and the sliding bottom cover. Two types of boxes were used in loading tests of grouted organic soil samples. The square test boxes ($750 \times 750 \times 450\ mm^3$) and rectangular test boxes ($750 \times 1000 \times 450\ mm^3$) are shown in Fig. 7. The thickness of the steel was chosen as 8 mm to ensure rigid boundary conditions. A sandbox (filled with sand) was placed below these sampling boxes to mimic the silty sand layer.

The top cover of the boxes was strengthened to prevent self-yielding while being pushed into the soil using force. The top cover also contained holes so the trapped air could be removed when the box is uniaxially pushed down. The edges of the box at the bottom were deformed to have an angle of 30° to encourage a knife effect and easier insertion into the soil without significant disturbance. After placing the box in the soil, a movable bottom cover slided sideways to close the box, and thus, undisturbed organic soil samples were collected to represent the site conditions.

The jet grout setup used in this study was designed by the authors. The jet grouting setup comprised a mixing tank (cement and water), a high-pressure pump, drilling rods with different nozzle diameters, some grout-injection accessories, and the control unit. The selection of the pneumatic pump is crucial because it directly influences the viscosity of the grout. While the rod was allowed rotational and transitional movement, the lifting and rotating speeds could also be controlled. While Fig. 8a shows the jet grouting device and its dimensions, the rear view with the steel test box installed can be seen in Fig. 8b.

2.4 Testing Procedure

Figure 9 shows the formation procedure of JGCs. As mentioned before, the water/cement ratio was chosen as 1:1 for all JGCs.

The optimization process aims to obtain soilcrete columns of 60 mm diameter and 450 mm length. Various attempts were made to optimize the dimensions of the soilcrete columns by altering the rotating speed, lifting speed, and injection pressures as shown in Fig. 10. Images were obtained after removing the columns from the soil and tagged based on the number of experiments as JGCa, JGCb, JGCc, JGCd, JGCe, JGCf, and JGCg as shown in Fig. 10.

The details about the parameters for the production of each column (shown in Fig. 10a–g) are given Table 5.

Since the JGCg is dimensionally accurate, the installation process was completed using the parameters used for JCGg (nozzle diameter = 1.5 mm, grout pressure = 5 bar, rotating speed = 27 mm/s, lifting speed = 2.4 mm/s). After the installation of the columns, the boxes were wrapped with a Nylon cover to preserve the moisture content. Later, boxes were cured at 24 °C for 28 days, followed by the loading tests.

The loading tests are conducted using the sandbox and test box to place the latter on the former. The dimensions of both types of boxes are given in Fig. 7b, and d. Literature

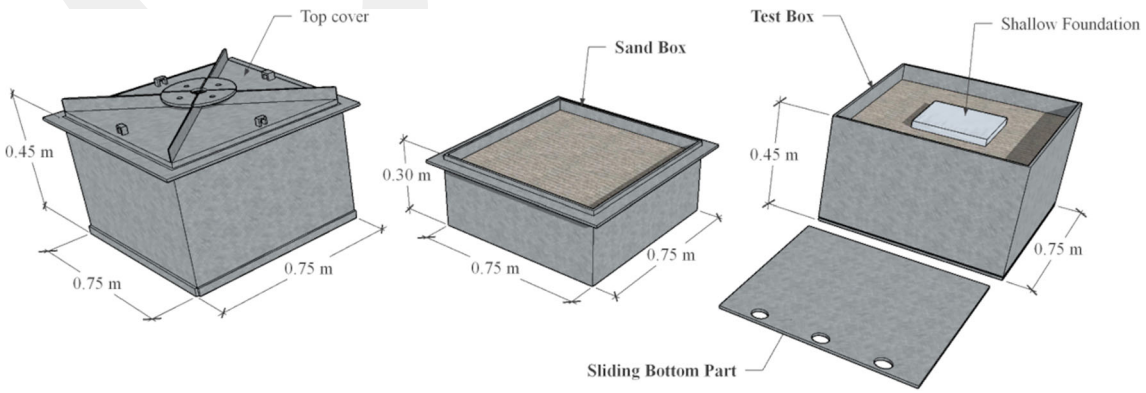

Fig. 7 Details of model test boxes used for undisturbed sampling

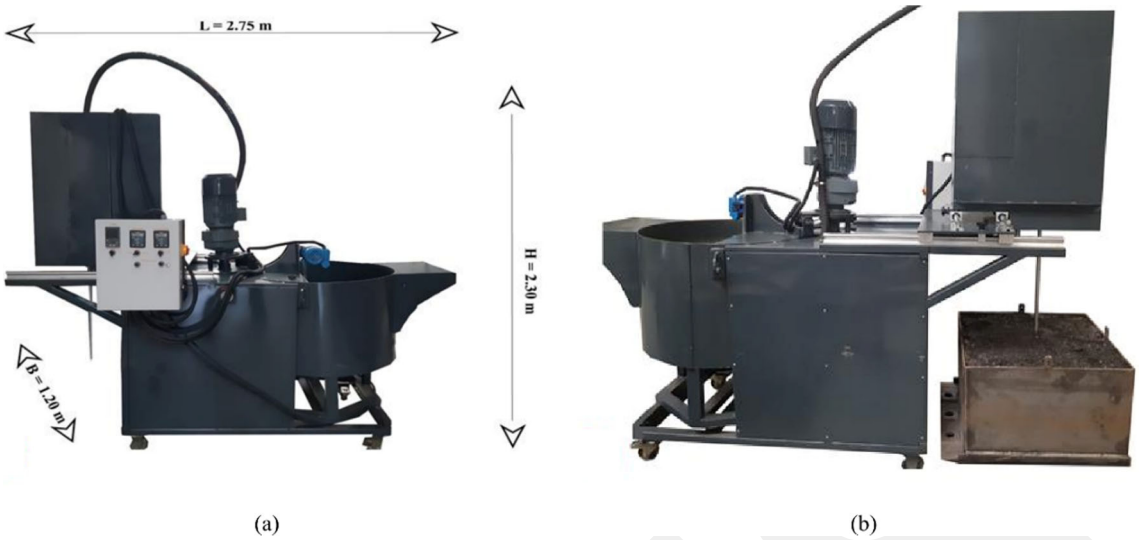

Fig. 8 **a** Front view and **b** Rear view of the domestically designed lab-scale jet grouting device

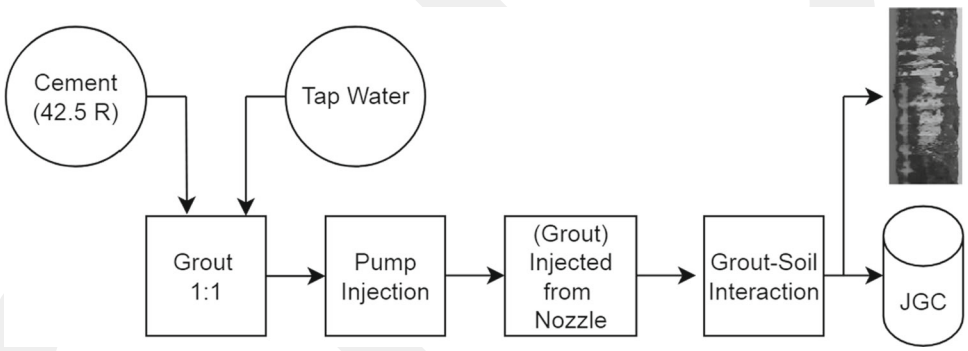

Fig. 9 Schematic diagram of formation procedure of JGCs

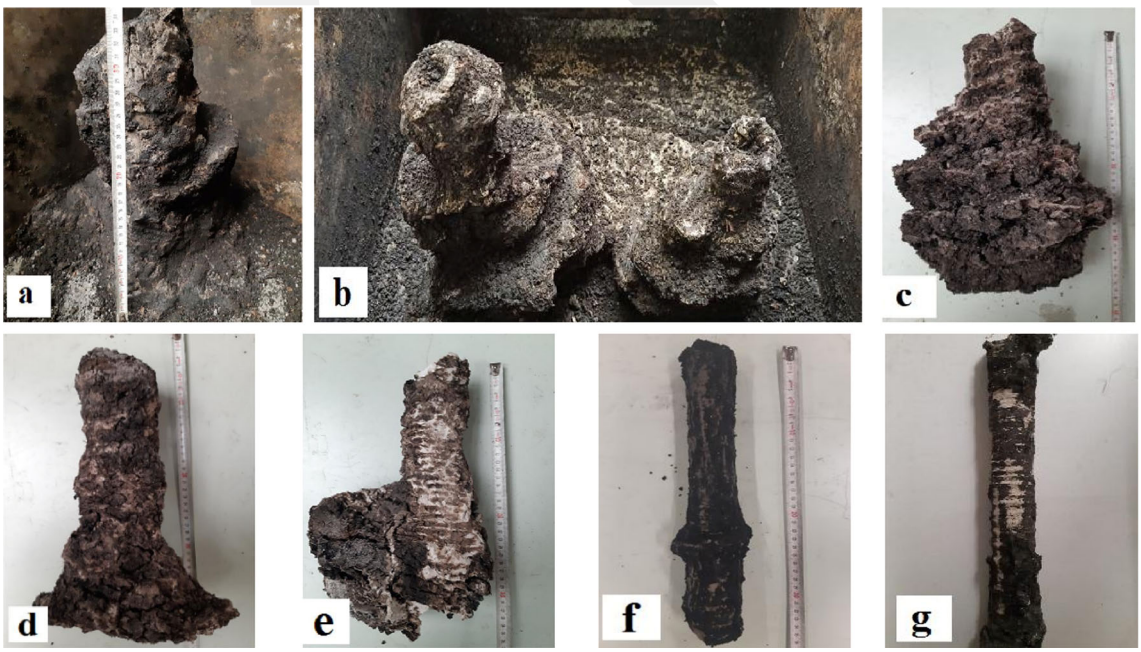

Fig. 10 **a**–**g** The formation process of all soilcrete columns during optimization

Table 5 Properties of JGCs and their dimensions

Column name	Nozzle Diameter (mm)	Grout pressure, p (bar)	Rotating speed (mm/s)	Lifting speed (mm/s)	Mean diameter of column (mm)	Column height (mm)
JGCa	1.5	6.00	23.0	2.20	150	350
JGCb	1.5	9.00	19.0	3.20	200	400
JGCc	1.5	10.00	21.0	3.00	200	360
JGCd	1.5	6.00	23.0	2.00	160	410
JGCe	1.5	8.00	20.0	3.20	220	450
JGCf	1.5	6.00	23.0	2.80	60	450
JGCg	1.5	5.00	27.0	2.40	60	450

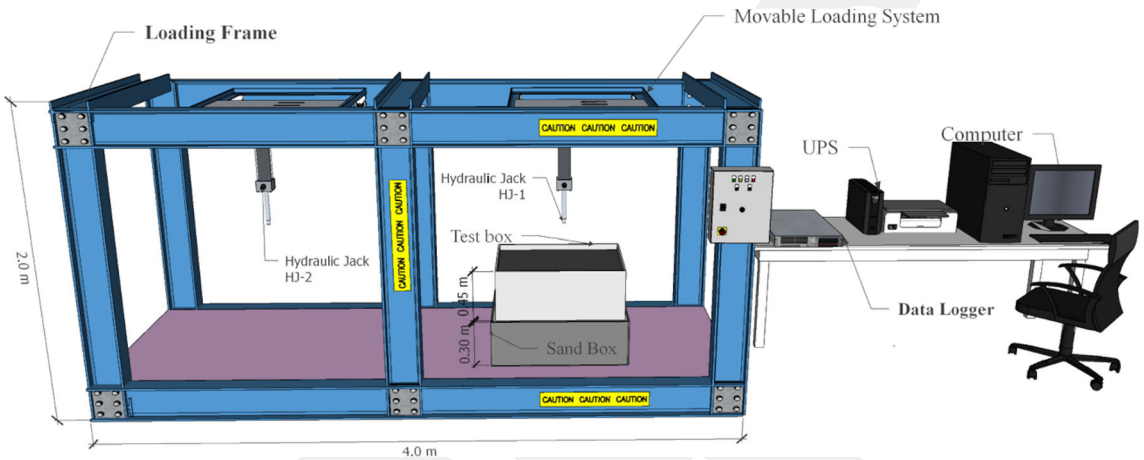

Fig. 11 3D test setup and view of the loading frame

suggests a sand thickness of 0.7D–4.0D (D = diameter of the column) under the column; therefore, the thickness of the sand layer was chosen as 300 mm [42]. The sand layer was compacted in 5 layers at a relative density of $D_r = 60\%$. A 100-kN loading frame system was used with a hydraulic jack and displacement and load control unit. The loading rate of the hydraulic jack could be changed between 0.5 and 10 mm/min. An S-type load cell with a capacity of 50 kN was just below the hydraulic jack. 16-channel data logger connected the measurement elements, such as the load cell, and linear variable differential transformers (LVDTs) were located under the load cell. In addition, on the left side of the frame system, there is a horizontal crane system with a capacity of 30 kN to remove the bottom cover; hence the OS and sand form the top layer of the model experiment. The studies carried out during the execution of model experiments in the frame system are presented in Fig. 11.

Two types of box setups were used for the experiments: square boxes (750 × 750 × 750 mm^3) and rectangular boxes (750 × 1000 × 750 mm^3). Within both setups, the upper box contained the undisturbed organic soil (Layer-1) collected from the site, and the lower box contained sand (Layer-2). The sand was placed to mimic the site conditions during the experiments in the laboratory.

The upper boxes in both configurations were covered with rigid steel plates of 20 mm thickness. The other dimensions of the plate were selected as 240 × 240 mm^2 and 80 × 240 mm^2 for 2 × 2 JGCs and 80 × 240 mm^2 configuration, respectively.

Single JGCs and groups of JGCs were formed in OS using a laboratory-scale JG device. The JGCs were formed at three different spacing and diameter ratios (S/D: 2.0, 2.5, 3.0), where 'S' is the distance between the center of JGCs and 'D' is the diameter of the JGC. For each experiment, the JGCs were constructed considering the square and strip pattern with a diameter of 60 mm and a length of 450 mm.

Soil pressure sensors (2 MPa capacity) were placed inside the boxes and close to the edges to check boundary conditions. According to the soil pressure calibration certificate taken from the supplier, the sensitivity of the soil pressure is less than or equal to 0.005%; this means 1 kPa sensitivity is possible when 2 MPa capacity is used. Negligible stress levels were measured using the four soil pressure sensors installed perpendicular to the four sides of the boxes. This proves that the frame sizes determined from the preliminary studies are

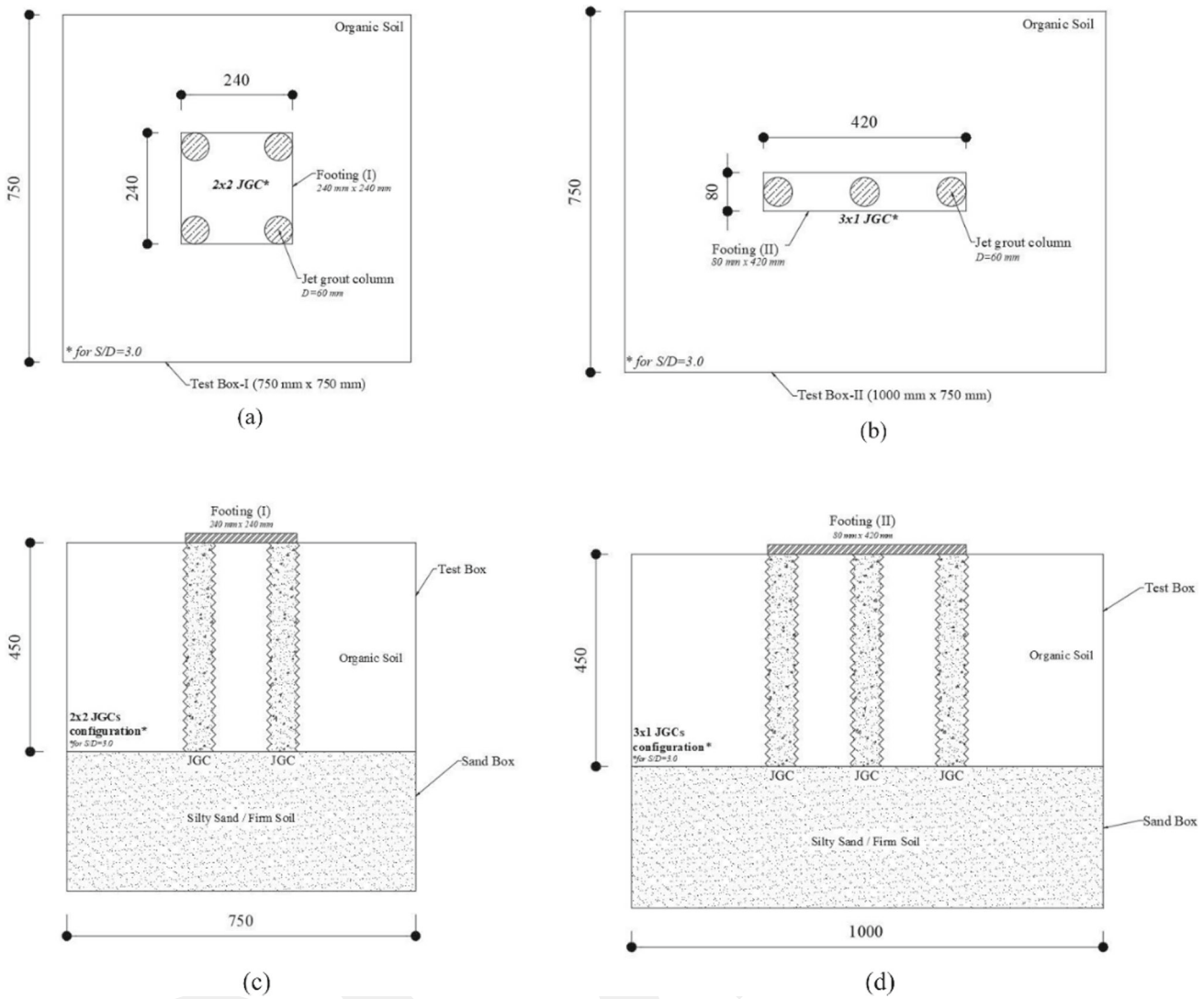

Fig. 12 **a**, **b** Plan view of 2 × 2 JGC and 3 × 1 JGC **c**, **d** Cross section view of 2 × 2 JGC and 3 × 1 JGC

sufficient. All sides of the test box were solidly fixed to prevent lateral displacement during loading. To reduce the effect of side-wall friction, the inner side of the test box walls was lubricated. In the study, two LVDTs (100 mm vertical displacement capacity) are placed on both sides of the plates, and the average settlement value is given in the related graphs. The loading rate was defined as 1.0 mm/min, which is compatible with previous studies on expansive soil [43, 44]. All tests were simulated with a numerical model and analyzed. The schematics of the improved soil with soilcrete columns, box dimensions, footings, and cross sections can be seen in Fig. 12. The square and strip rigid plates represent square footing (SQF) and strip footing (STF), respectively.

The index properties of OS taken from the center of each box were determined at the end of the experiments, considering that there may be changes in the geotechnical properties. The results are given in Table 6, which show that the values of index properties were close to each other.

These findings indicate an approximately uniform structure with the study area and laboratory samples.

In this study, the bearing capacity of the unreinforced OS was obtained in the loading test. Then, for a single JGC, the square and strip footings were placed in the OS, and second-group loading tests were carried out. Finally, third-group loading tests were carried out for square and strip footings placed on JGCs formed by group columns with different spacings (*S*/*D*: 2.0, 2.5, 3.0). Figure 13 shows the loading test arrangement for the square and rectangular test boxes before and after the loading, respectively. All loading tests ended when the ultimate peak strength or displacement conditions were reached, which meant no more load increase was observed.

Table 6 Geotechnical properties of organic soil after the laboratory model experiments

Index properties	Organic soil	Single column	$S/D = 2.0$	$S/D = 2.5$	$S/D = 3.0$
Unit weight (γ_s, kN/m^3)	18.20	18.32	19.10	19.20	18.80
Moisture content (w, %)	182.8	176.3	184.8	173.8	167.8
Liquid limit (w_L, %)	208.9	201.2	203.2	207.2	211.2
Plastic limit (w_P, %)	95.6	98.3	102.1	101.9	104.5
Plasticity index (I_P, %)	113.3	102.9	102.9	105.3	106.7

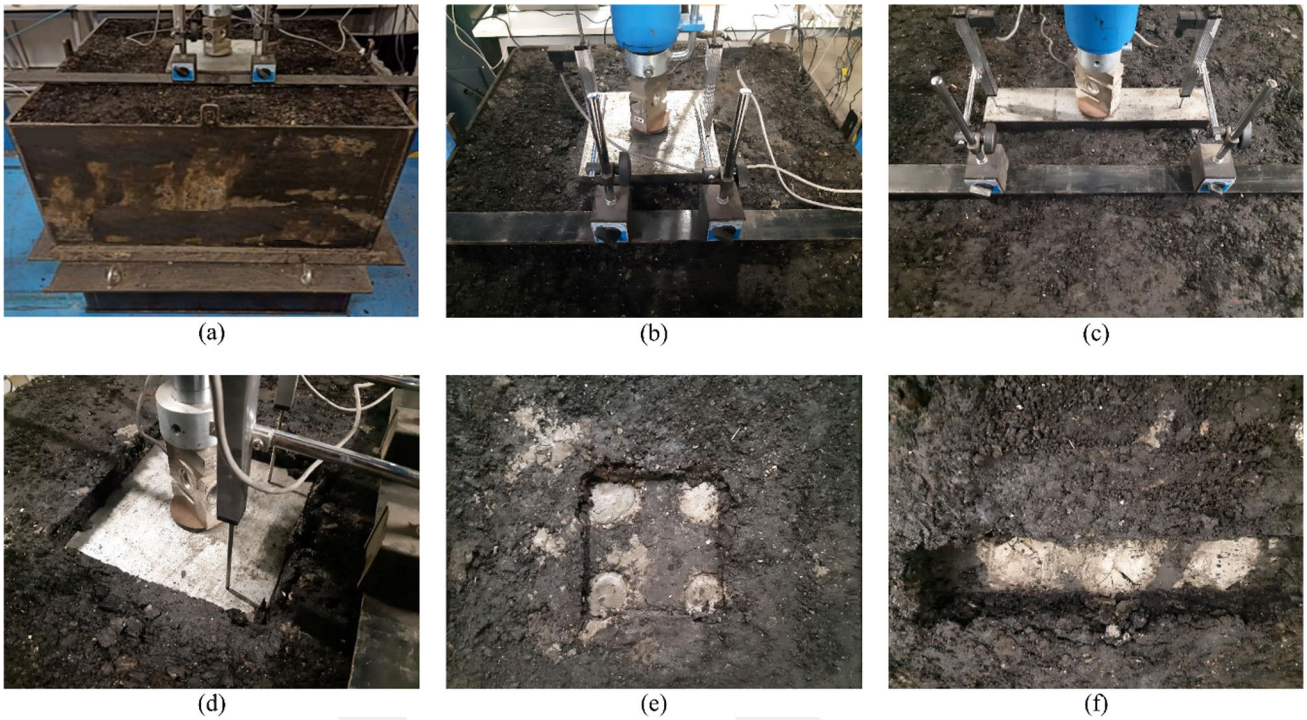

Fig. 13 Loading test arrangement for square test box (**a**), the position of 240 mm × 240 mm square footing and LVDTs before the test (**b**), the position of 8 mm × 420 mm rectangular footing and LVDTs before the test (**c**), the position of square footing after the loading (**d**), the top view of 2 × 2 JGCs configuration after the loading (**e**), the top view of 3 × 1 JGCs configuration after the loading (**f**)

3 Numerical Modeling

Geotechnical softwares are specialized tools for modeling soil behavior and providing solutions for most geotechnical tasks. New softwares for geotechnical purposes are constantly being introduced and developed [45]. In this study, PLAXIS 3D software was used for simulating the model experiments and determining the foundation settlement and bearing capacity of the soil [46]. The numerical model's calibration enabled the observation of obtained load settlement curves that closely matched the results of the laboratory model under vertical load testing. Further numerical assessments for a larger group of jet grouting columns can be performed by obtaining a pile load test on the site. Finite element (FE) analyses were performed for the unimproved OS, and group JGCs were used as the reinforcement of soft soil. The geotechnical characteristics of the soil must be defined in the model to simulate time-dependent and nonlinear soil behavior [47, 48]. In PLAXIS 3D, soft soil and soft soil creep material models are recommended for the modeling of peat soils. The SSC model is preferable when creep or secondary (time-dependent) compression is considered. This study focused on interpreting the bearing capacity behavior in an undrained condition. Since secondary consolidation analyses were not considered during the current experiments (due to the longevity of secondary compression), the SS model was adopted [46, 49].

Additionally, the material manual of PLAXIS 3D suggests that near-normally consolidated clays, clayey silts, and peat may be modeled using the SS model. Such soils have a high degree of compressibility; therefore, oedometer tests were performed. As a result, modified compression index (λ^*) and

Table 7 Soil model types and parameters for numerical analysis

Material properties	Organic soil	Silty sand	Jet grout columns
Material model	Soft soil	Mohr–Coulomb	Mohr–Coulomb
Young's modulus, E (kPa)	–	15×10^3	5×10^5
Poisson's ratio, ν	–	0.30	0.25
Cohesion, c (kPa)	9.70	10.70	900
Friction angle, ϕ (degree)	29.80	41.20	0
Dilatancy angle, Ψ (degree)	–	0	0
λ (Lambda)	0.20	–	–
κ (Kappa)	0.04	–	–

modified swelling index (κ^*) values were obtained. Direct shear tests were performed to get the strength parameters of OS. The material properties and other relevant parameters of the OS and silty sand used in the numerical analysis are given in Table 7.

Similar to many studies in the literature [50–53], the linear elastic, perfectly plastic model (Mohr–Coulomb) was used to represent the soil and JGC behavior in the numerical analyses. The input parameters for the FE analysis of soil/cement columns have been adopted from the study by Han et al. and Yi et al. [54, 55]. Interface elements were set between the soilcrete column and the surrounding OS. Applying an interface reduction factor $R_{\text{inter}} = 1$, the interaction between JGCs and the surrounding soil can be assumed as rigid. The basic soil elements were the 10-node quadratic tetrahedral elements. The bearing capacity of soil, which is modeled using medium mesh and fine mesh, rarely differs. This is in accordance with findings of Broere and van Tol [56]. Wehnert and Vermeer suggest utilization of an interface element between the pile and the soil to achieve reliable findings [57]. Under and around the loading area, finer elements were used, and medium meshes were used near the lateral boundaries. When gravity loading is used, the soil layers have no initial stresses at the start of the calculations. In the first calculation phase, the stresses are produced by adding the soil self-weight. This was achieved by plastic calculation by setting the loading input as the total multiplier and M_{weight} as 1.0. After the initial stresses, the displacements were reset to zero at the beginning of the calculation phase.

4 Results and Discussion

4.1 Experimental Results

In this study, since no significant bearing capacity can be obtained from the vertical load–settlement curves, the 0.1B method was used to determine the bearing capacity of unimproved organic soil [58]. In this method, the bearing capacity of soil is obtained from the stress value corresponding to the 0.1B (one-tenth of the footing width) settlement value. The vertical loads applied to all soilcrete columns, and the ultimate bearing capacities were determined by analyzing the load–settlement curves obtained from the loading tests. The graphical methods developed by Brinch Hansen, De Beer and Wallays, and the double tangent approach were used to determine the ultimate bearing capacities [59–61]. Brinch Hansen proposed that ultimate pile capacity must be defined as the load that gives four times the pile head settlement attained for 80% of the load. The '80% criterion' can be calculated directly from the load–settlement curve; however, it is more precisely established by plotting the square root of each settlement value divided by its load value against the settlement. After a certain point, the graph continues linearly. The load–settlement graph is drawn on a logarithmic scale for both axes in the De Beer and Wallays technique. The points on the graph are located around the straight lines on the different slopes if the load applied to the test pile passes the ultimate load. The slope of these straight lines has no result, but the point where they intersect is the point at which the pile's reaction to the applied load changes and the load that corresponds to this point is the ultimate load. The ultimate bearing capacity of piles can be estimated using the double tangent method by drawing the first tangent lines to the starting and ending portions of the load–settlement curves. The junction point of these two tangents represents the ultimate bearing capacity of the pile. An improvement factor (IF), which is the ratio of the bearing capacity of grouted soil to that of the unimproved soil, is given to express the improvement rate. A comparison of calculated and measured ultimate bearing capacity of soilcrete columns and IF can be seen in Table 8.

The IF values obtained using tangent methods are 1.62–1.69 for single JGCs, 3.57–4.27 for group column-SQF, and 3.84–4.73 for group column-STF. According to Table 8, the OS bearing capacity increased approximately 1.70, 3.50–4.50, and 3.80–5.00 times for a single JGC, a group column-SQF, and a group column-STF, respectively. Although the JGCs have the same diameter and length, the corresponding IF values vary considerably. In general, the vertical displacement of 10% of the column diameter is crucial for the calculation of the bearing capacity of improved OS. Therefore, nearly 6–7 mm settlement value is considered in the comparison since the column diameters were

Table 8 Comparison of calculated and measured ultimate bearing capacity of soilcrete columns

Soilcrete column info	Brinch Hansen 80%	De Beer and Wallays	PLAXIS 3D	Measured double tangent method	IF (Improvement factor)
	All units in kPa				
Unimproved OS (STF)*	–	–	71	82	–
Unimproved OS (SQF)*	–	–	87	94	–
Single JGC (STF)	147	156	127	139	1.69
Single JGC (SQF)	158	171	133	152	1.62
Group column $S/D = 2.0$ (STF)	352	331	311	315	3.84
Group column $S/D = 2.0$ (SQF)	364	355	325	336	3.57
Group column $S/D = 2.5$ (STF)	370	349	337	342	4.17
Group column $S/D = 2.5$ (SQF)	407	399	361	376	4.00
Group column $S/D = 3.0$ (STF)	427	402	376	388	4.73
Group column $S/D = 3.0$ (SQF)	442	416	389	401	4.27

*The bearing capacity of unimproved OS (STF) and unimproved OS (SQF) were calculated by 0.1B method

60 mm [62]. Figure 14 illustrates the vertical load and settlement curves of JGC in natural OS. The ultimate vertical load value of the strip foundation for natural OS was about 1.43 kN. After placing jet grout columns with $S/D = 2.0$ and 2.5 intervals under the square foundation, the ultimate vertical load values for the square foundation were obtained as 2.30 and 3.40 kN, respectively. As for the strip foundation, the ultimate vertical load values were obtained as 2.45 and 3.45 kN for $S/D = 2.0$ and 2.5 intervals, respectively. The vertical load value of STF at 6.0 mm settlement was 4.64 kN for $S/D = 3.0$. This value increased further and reached 7 kN at 10 mm settlement. The shape of the curves obtained in Fig. 14a for SQF was similar to those obtained in Fig. 14b. The soilcrete columns increased the bearing capacity of OS 2.5–4.0 times for square foundation and 3.0–4.5 times for strip foundation. The $S/D = 3.0$ ratio gives the highest bearing capacity for both foundation types. The loadings were not stopped at 6 mm settlement and continued until the JGCs reached the peak stresses.

The loading of soilcrete columns was conducted to obtain the ultimate bearing capacity. The tests were terminated when the load started decreasing, and the settlement continued to increase. The ultimate bearing capacity of the soilcrete column was defined when a large displacement was observed at the soilcrete column's head. In Fig. 15, the relationship between soilcrete head load vs. soilcrete head settlement and applied stress vs. settlement for square and rectangular test boxes was given, respectively.

The OS settlement goes up to 100 mm, and there is no peak point since the failure type is punching. However, the failure type of improved soil with JGCs settlement curves shows general shear failure. In both boxes, the group column with $S/D = 3.0$ reached the highest ultimate bearing capacity. This finding might be correct because the influence lines of $S/D = 2.0$ and $S/D = 2.5$ overlapped. Therefore, this highly stressed zone reduced the bearing capacity for $S/D = 2.0$ and $S/D = 2.5$ ratios. Group columns provide a higher bearing capacity than single columns for improving the bearing capacity and strength of problematic peat soils because group columns work as a block, and failure is dependent on skin friction along the group columns' periphery and end-bearing.

The deep soil stabilization process not only forms a soil column but also stabilizes the surrounding soil, increasing the bearing capacity by increasing adhesion between the soil column and the surrounding stabilized soil.

In the numerical simulation, three soil–cement columns were placed in a 3×1 JGCs configuration, and four soil–cement columns were placed in a 2×2 JGCs configuration. The JGC head load–JGC head settlement curves of model tests and FE analyses results can be seen in Fig. 16. The comparison of the curves indicates that they follow a similar trend. It can be seen that the results of the FE analysis and model tests results are identical. In general, the bearing capacity values obtained by the numerical analysis using medium meshing were nearly 10% lower than the model experiments. However, fine meshing analyses converged to experimental curves

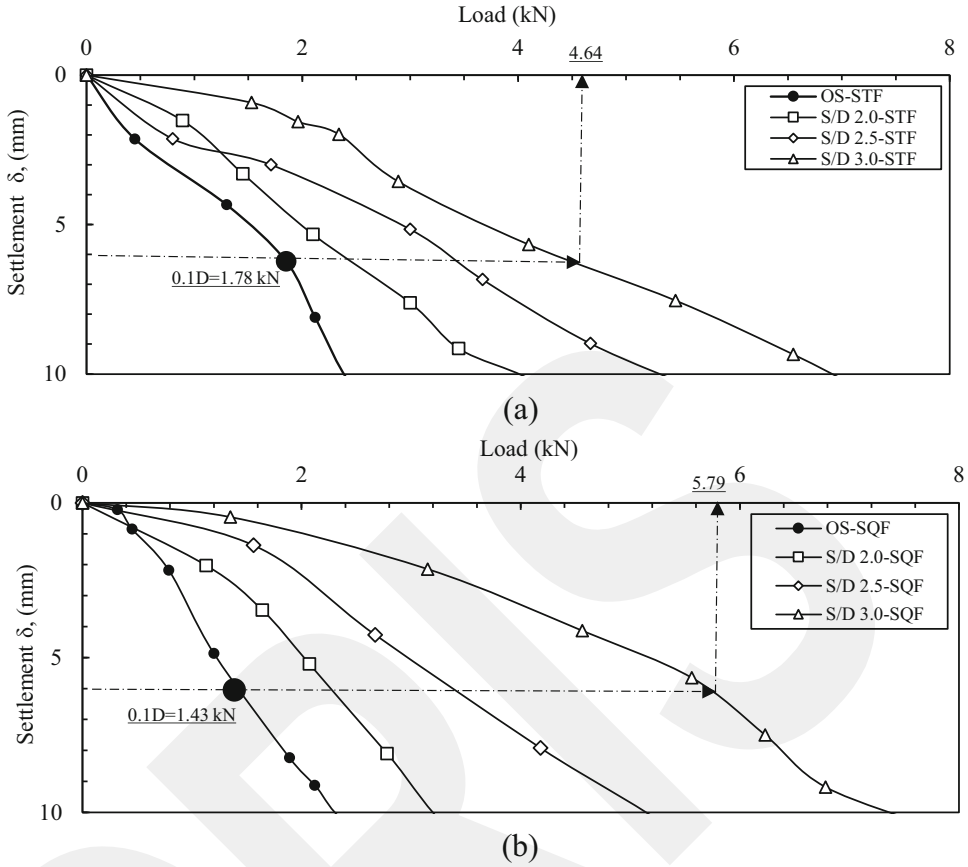

Fig. 14 Load–settlement curves of OS and improved soil in the square test box (**a**) and the rectangular test box (**b**)

within the 5–10% difference range. The numerical analysis results are lower because the PLAXIS 3D program's input parameters do not adequately account for the influence of the soil's intact fibers and the voids created by ruined fiber and plant residues on the engineering qualities of the soil.

As a result, it is thought that the FE analysis findings are accurate and reliable for estimating the bearing capacity of OS. After the loadings were removed, half of the test boxes were excavated to expose the side views of the columns, as shown in Fig. 17. When the JGCs reached their ultimate load capacity, the cracks of the columns generally occurred between $L/4$ and $L/3$ from the surface. This is because the load and stress are primarily concentrated in that region. Additionally, it was observed that there was no leaning of columns from the vertical axis.

It was observed that the OS in the box tends to swell up to 60% of the settlement in the unimproved condition and the range of 40% to 45% of settlement in the improved condition after the unloading. This observation can be explained by the fact that the ruined and undisturbed plants and animals remain in the organic soil giving the soil an elastic structure. Consequently, a movement in the opposite direction of settlement occurs when the soil is unloaded. The soilcrete samples were removed from the OS after the loading tests. The samples were cut with the concrete saw without disturbance to perform a compressive strength test (Fig. 18). The core samples were prepared as a length/diameter ratio of $L/D = 2$ with an average diameter value of 60 mm.

The uniaxial compressive strength tests of the cylindrical concrete specimen were performed for three JGC samples for each loading group according to ASTM D1633. The resultant average strength values for 28 days are listed in Table 9 [63].

The compressive load was applied continuously at a rate of 0.3 MPa/s until the ultimate peak strength was reached. Because the column is an in situ mixture of cement, water, and soil, the compressive strength properties are determined mainly by the nature and composition of the soil. The moisture content of the soil may raise the water/cement ratio of the soilcrete, hence lowering its compressive strength. Moreover, the compressive strength may decrease due to the organic soil's high moisture content (194%) of plant and fiber remains. These columns are called soilcrete since the columns consist of cement and soil. There are two soil layers in the current study's test box: OS and silty sand. According to Table 9, the average compressive strength value of the JGCs samples (5.1 MPa) is between the limits and closer to the upper limit for peats and clay soils, which is suggested by Stoel and given in Table 10 for different soil types based on the ground conditions [64]. Wang mentioned that a field study in Seoul proved that after 28 days of curing to grout $W/C = 1$

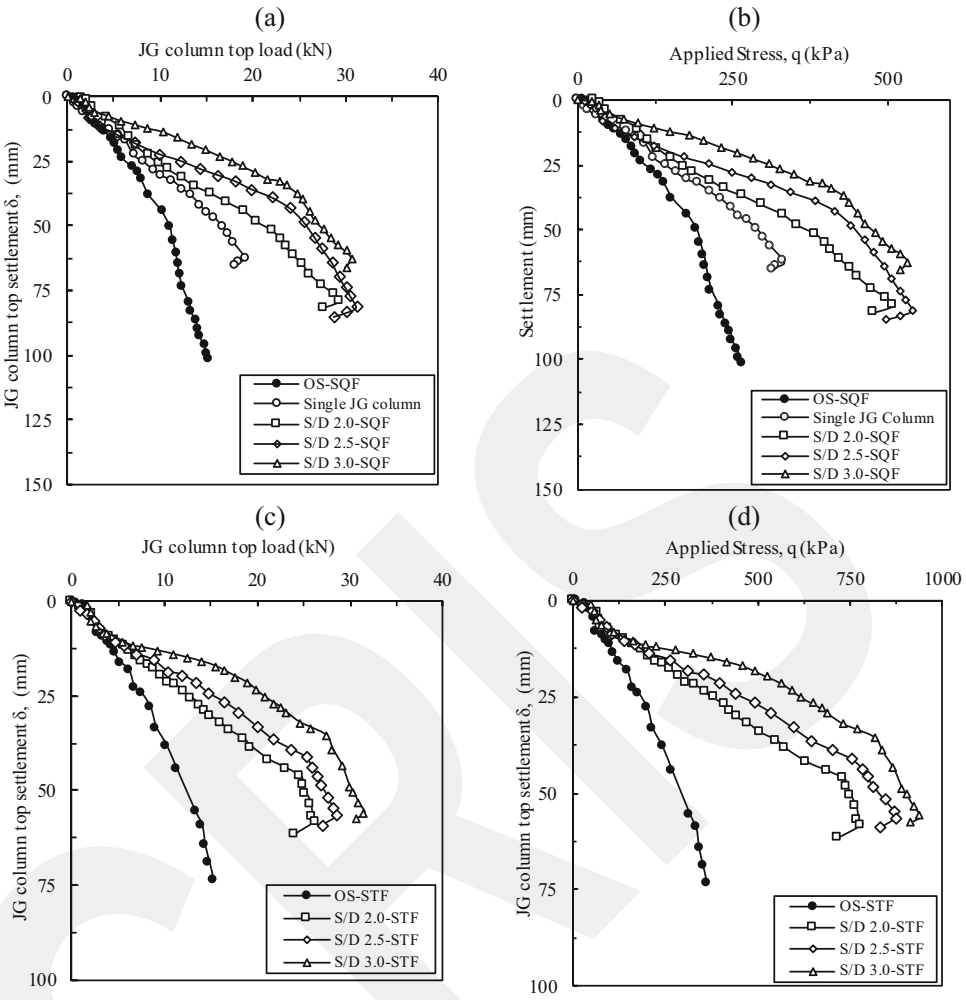

Fig. 15 Load–settlement and stress–settlement curves of improved organic soil inside square test boxes (**a**, **b**) and rectangular test boxes (**c**, **d**)

by weight, the unconfined compressive strength of the JGCs may reach 5.0–6.0 MPa [65]. Another field study shows that the unconfined compressive strength of JGCs can vary from 2.78 to 5.52 MPa [66]. A field study that includes five different sites improved with JGCs revealed that the unconfined compressive strengths were between 1.54 and 6.70 MPa [67].

4.2 Numerical Results

The appropriate mesh size is vital in numerical modeling since the mesh's quality increases the analyses' accuracy. A convergence study was carried out to select mesh size. The computing effort has therefore been minimized. A very fine mesh was employed at the stress concentration zone, and mesh refinement was performed toward the edges, from coarse mesh to very fine mesh. Vertical cross-sectional and horizontal cross-sectional views for square footing (SQF) and strip footing (STF) are given in Fig. 19.

As shown in Fig. 19, the total displacement contours have not reached the edges of the boxes for both vertical and horizontal cross sections; therefore, there is no boundary condition. Considering the vertical stress concentrations for OS, the contours are denser near the surface. Cracks in the columns were observed in this zone at the end of the axial loading test. The $S/D = 2.0$ value has a very close gap between columns; due to these conditions, stress bulbs may overlap; hence, the bearing capacity for $S/D = 2.0$ is a little bit low compared to other spacing ratios. Fine and very fine meshing at the stress concentration region (plates, column, and surrounding soil) resulted in the convergence between experimental and numerical study curves. Fine meshing resulted in more compatibility with the model test curve; however, there is not too much difference from medium meshing because using an interface element between the footing, column, and surrounding soil lower the dependence of the calculated end resistance.

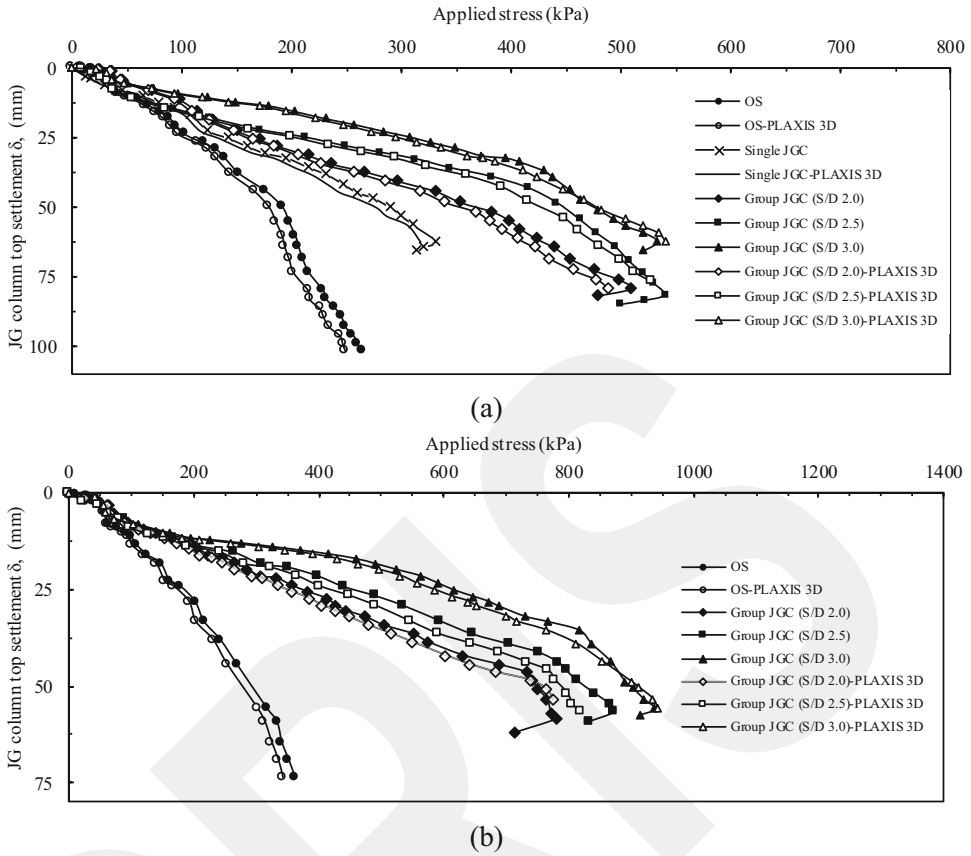

Fig. 16 Applied stress and settlement results of the model loading tests and numerical analysis **a** square test box and **b** rectangle test box

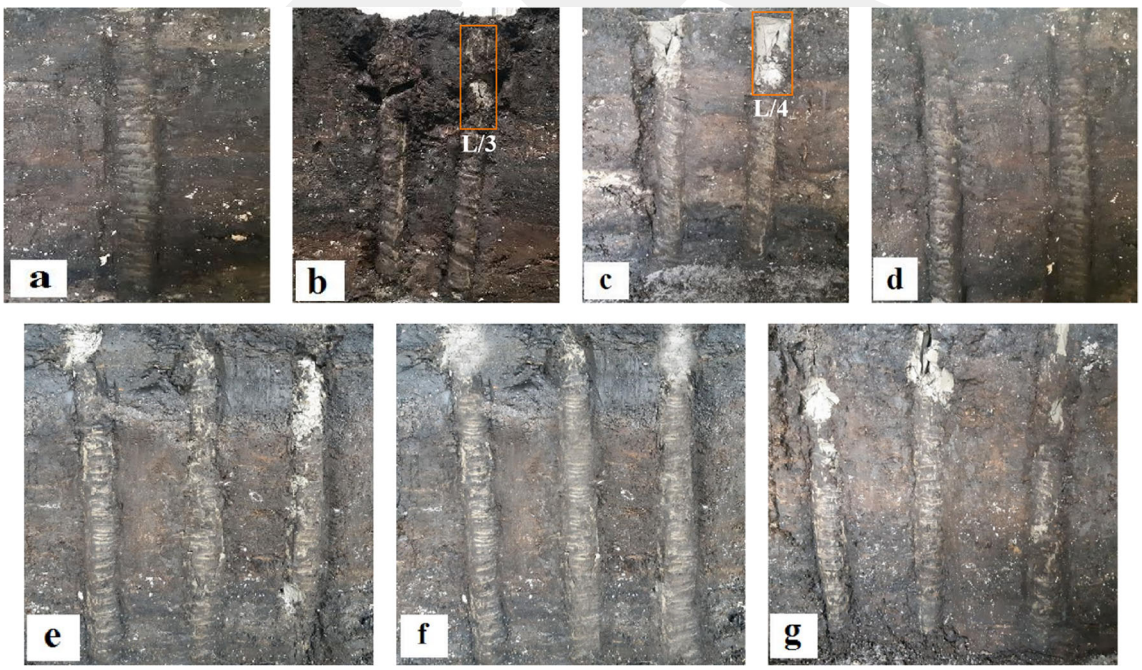

Fig. 17 The cross sections of the boxes: **a** single JGC, **b** $S/D = 2.0$ square JGCs, **c** $S/D = 2.5$ square JGCs, **d** $S/D = 3.0$ square JGCs, **e** $S/D = 2.0$ rectangle JGCs, **f** $S/D = 2.5$ rectangle JGCs, **g** $S/D = 3.0$ rectangle JGCs

Fig. 18 Uniaxial compressive strength test on excavated soilcrete samples

5 Conclusion

Jet grouting is a convenient solution to many geotechnical problems and is widely used as a soil improvement technique. The physical modeling of the jet grouting mechanism was investigated in this study. The authors designed a jet grout device and fabricated to construct the test-scale columns. The present study is limited to the model test on end-bearing soilcrete columns, simulating a site scenario where the columns go down to silty sand. The floating column behavior was not investigated. Additionally, developing a theoretical model to predict bearing capacity can be done by expanding the number of tests and the number of analyzed parameters. The current study is bound by time constraints and the limited number of undisturbed samples.

Field study, large-scale model tests, and dimensional analyses are recommended before using the results of the present study in site applications. The following conclusions are drawn due to the improvement of the OS and the laboratory studies.

- Group columns provide a higher value than single columns for improving problematic peat soils' bearing capacity and strength.
- The highest bearing capacity value is observed when $S/D = 3.0$ for both JGCs configurations.
- The failure mechanism of the soil and columns were visualized after the loading tests. The cracks were observed at a distance from the soil surface $L/4$ between $L/3$ of columns because the stress contours are denser in this area.
- The bearing capacity values obtained by the numerical analysis using fine meshing were nearly 5% lower than the model experiments.

It is believed that organic soil removed from the site without being disturbed can be improved using soilcrete columns

Table 9 Compressive strength values of excavated JGCs

Sample type	JG Sample 1 Strength (MPa)	JG sample 2 Strength (MPa)	JG sample 3 Strength (MPa)	Mean Strength (MPa)
Single column	4.9	5.4	4.6	4.9
$S/D = 2.0$ Square footing	5.8	4.6	5.5	5.3
$S/D = 2.5$ Square footing	5.2	5.3	5.7	5.4
$S/D = 3.0$ Square footing	4.7	5.4	5.1	5.1
$S/D = 2.0$ Strip footing	5.1	5.6	5.7	5.5
$S/D = 2.5$ Strip footing	5.6	5.2	5.5	5.4
$S/D = 3.0$ Strip footing	5.3	5.1	4.5	5.0

Table 10 Typical average uniaxial compressive strengths of jet-grouted soils according to Stoel [64]

Soil type	UCS (MPa)	
	Lower limit	Upper limit
Peat	1.0	6.0
Clay	3.0	7.0
Silt	5.0	15.0
Sand	10.0	40.0
Gravel	10.0	40.0

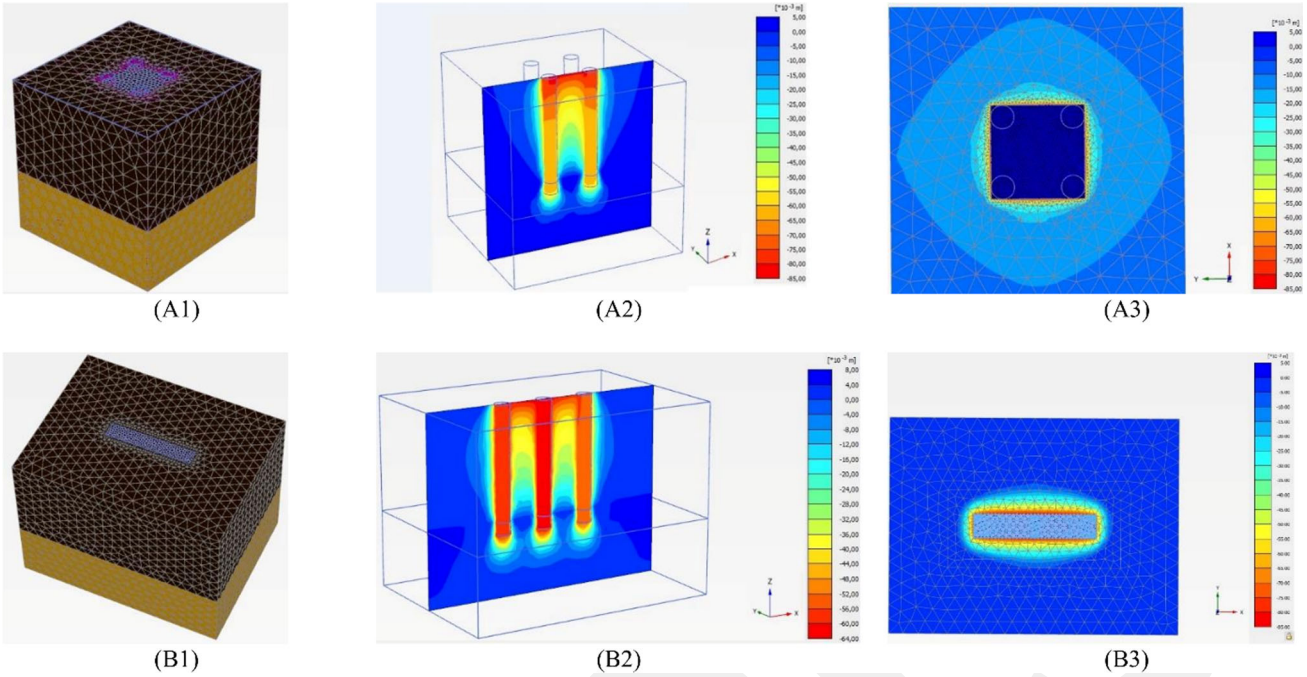

Fig. 19 Fine meshing, vertical cross-sectional views, and total displacements of the soilcrete columns after numerical analyses with PLAXIS 3D for 2 × 2 JGC *S*/*D* = 3.0 SQF (A1–A2–A3) and 3 × 1 JGC *S*/*D* = 3.0 STF (B1–B2–B3)

according to the results of model tests and numerical analyses, but the correct spacing should be defined by considering the soil's geotechnical parameters. It should be remembered that numerical analysis results in these organic soil sites can be helpful for early evaluation. Still, choosing the correct parameters for the analysis programs is crucial.

Acknowledgements This study was funded through the "The Scientific and Technological Research Council of Turkey" (TUBİTAK). Project Type; The Scientific and Technological Research Projects Funding Program (1001) and Project No.:119M974).

Author Contribution HY did conceptualization, methodology, experimental program, writing—original draft preparation. ZK done supervision, validation, writing–reviewing and editing. CCÇ performed methodology, experimental program, writing—original draft preparation. EU was involved in experimental program, methodology, reviewing and editing, and software. AE contributed to conceptualization, methodology, experimental program, writing—original draft preparation. MA done methodology, reviewing, and editing.

Data Availability All data, models, and code generated or used during the study appear in the submitted article. Some or all data, models, or code that support the findings of this study are available from the corresponding author upon reasonable request.

Declarations

Conflict of interest The authors declare that they have no known competing financial interests or personal relationships that could have appeared to influence the work reported in this paper.

References

1. Dehghanbanadaki, A.; Sotoudeh, M.; Golpazir, I.; Keshtkarbanaeemoghadam, A.; Ilbeigi, M.: Prediction of geotechnical properties of treated fibrous peat by artificial neural networks. Predict. Geotech. Prop. Treat. **78**, 1345–1358 (2019)
2. Paul, A.; Hussain, M.: An experiential investigation on the compressibility behavior of cement-treated Indian peat. Bull. Eng. Geol. Environ. **79**, 1471–1485 (2019)
3. Cao, X.; Yue, M.; Xu, H.; Chen, S.; Hou, Y.; Wang, X.: The technology and application of improving bearing capacity of deep peat soil subgrade. In: E3S Web of Conferences, p. 01010. EDP Sciences (2021)
4. Ulusay, R.; Tuncay, E.; Hasançebi, N.: Geo-engineering properties and settlement of peaty soils at an industrial site (Turkey). Bull. Eng. Geol. Environ. **69**, 397–410 (2010)
5. Canakci, H.; Hamed, M.; Celik, F.; Sidik, W.; Eviz, F.: Friction characteristics of organic soil with construction materials. Soils Found. **56**, 965–972 (2016). https://doi.org/10.1016/j.sandf.2016.11.002
6. Muntohar, A.; Rahman, M.; Hashim, R.; Islam, M.S.: A numerical study of ground improvement technique using group of soil-column on peat. Pertanika J. Sci. Technol. **21**, 625–634 (2013)
7. Heymann, G.; Clayton, C.R.I.: Block sampling of soil: some practical considerations. In: Geotechnics for Developing Africa, pp. 331–339. CRC Press (2021)
8. Bouassida, M.; de Buhan, P.; Dormieux, L.: Bearing capacity of a foundation resting on a soil reinforced by a group of columns. Géotechnique **45**, 25–34 (1995)
9. Dutta, S.; Mandal, J.: Model studies on encased fly ash column–geocell composite systems in soft clay. J. Hazardous Toxic Radioact. Waste **21**, 04017001 (2017)
10. Zarkiewicz, K.: Laboratory experiment of soil vertical displacement measurement near an axially loaded pile. In: IOP Conference Series: Materials Science and Engineering, p. 032012 (2019)

11. Brill, G.T.; Burke, G.K.; Ringen, A.R.: A ten-year perspective of jet grouting: advancements in applications and technology. In: Third International Conference on Grouting and Ground Treatment, pp. 218–235. American Society of Civil Engineers, New Orleans (2003)
12. Elsawwaf, M.; Azzam, W.; Elghrouby, N.: The effect of jet grouting on enhancing the lateral behavior of piled raft foundation in soft clay (numerical investigation). Adv. Geol. Geotech. Eng. Res. **5**, 24–39 (2023)
13. Kareem, R.; Al-Abbas, K.A.: Numerical analysis of soil strength improved by cement injection. Univ. Thi-Qar J. Eng. Sci. **12**, 38–42 (2022)
14. Moayed, R.Z.; Azini, E.: Evaluation of numerical modeling of jet grouting design using in situ loading test. Int. J. Geotech. Geol. Eng. **14**, 125–130 (2020)
15. ASTM International.: ASTM D1587-00 Standard Practice for Thin-Walled Tube Sampling of Soils for Geotechnical Purposes (2000)
16. Lunne, T.; Berre, T.; Strandvik, S.: Sample disturbance effects in soft low plastic Norwegian clay. In: Symposium on Recent Developments in Soil and Pavement Mechanics, pp. 81–102 (1997)
17. ASTM International.: D2435 Standard Test Methods for One-Dimensional Consolidation Properties of Soils Using Incremental Loading (2020)
18. Kaya, Z.; Erol, A.: Comparison of bearing capacities of undisturbed organic soils by empirical relations and 2D finite element analysis. Arab. J. Geosci. (2021). https://doi.org/10.1007/s12517-021-08364-w
19. Andresen, A.; Kolstad, P.: The NGI 54 mm samplers for undisturbed sampling of clays and representative sampling of coarser materials. In: Proceedings of the International Symposium on Soil Sampling, Singapore, pp. 13–21 (1979)
20. Karlsrud, K.; Hernandez-Martinez, F.G.: Strength and deformation properties of Norwegian clays from laboratory tests on high-quality block samples. Can. Geotech. J. **50**(12):1273–1293 (2013)
21. ASTM International.: D6951/D6951M-18 Standard Test Method for Use of the Dynamic Cone Penetrometer in Shallow Pavement Applications (2015)
22. ASTM International.: D2573 Standard Test Method for Field Vane Shear Test in Cohesive Soil (2008)
23. ASTM International: D421-85 Practice for Dry Preparation of Soil Samples for Particle-Size Analysis and Determination of Soil Constant. West Conshohocken, New York (1998)
24. ASTM International: D422-63 Standard Test Method for Particle-Size Analysis of Soils. West Conshohocken, New York (2007)
25. ASTM International.: D2974-00 Standard Test Methods for Moisture, Ash, and Organic Matter of Peat and Other Organic Soils (2000)
26. British Standard Institution.: BSI 1377 Part 2 Liquid Limit-Cone Penetrometer Method, London (1990)
27. ASTM International.: D2216-19 Standard Test Methods for Laboratory Determination of Water (Moisture) Content of Soil and Rock by Mass (2019)
28. ASTM International.: D854-14 Standard Test Methods for Specific Gravity of Soil Solids by Water Pycnometer (2014)
29. ASTM International: D4318-17 Standard Test Methods for Liquid Limit, Plastic Limit, and Plasticity Index of Soils. West Conshohocken, New York (2017)
30. ASTM International.: D2166-91 Standard Test Methods for Unconfined Compressive Strength of Cohesive Soil, Philadelphia (1994)
31. ASTM International.: D6528-07 Standard Test Method for Consolidated Undrained Direct Simple Shear Testing of Cohesive Soils, West Conshohocken (2007)
32. ASTM International.: D3080 Standard Test Method for Direct Shear Test of Soils Under Consolidated Drained Conditions, Philadelphia (1985)
33. ASTM International.: D2976-71 Standart Test Method for pH of Peat Materials (2004)
34. ASTM International.: D2487-17e1 Standard Practice for Classification of Soils for Engineering Purposes. Unified Soil Classification System (2017)
35. Amuda, A.; Sahdi, F.; Hasan, A.; Taib, S.; Mohamad, A.: Measurement of amorphous peat shear strength in the direct shear box at high displacement rates. Geotech. Geol. Eng. **37**, 1059–1072 (2019)
36. Landva, A.; La Rochelle, P.: Compressibility and shear strength characteristics of radforth peats. In: Jarrett, P.M. (ed.) Testing of Peats and Organic Soils, pp. 157–191. ASTM STP 820 (1983)
37. Den Haan, E.; Uriel, A.; Rafnsson, E.: Theme report 7: special problem soils/soft rocks. In: 11th European Conference on Soil Mechanics and Foundation Engineering, pp. 139–180 (1995)
38. Ulusay, R.; Tuncay, E.; Hasancebi, N.: Geo-engineering properties and settlement of peaty soils at an industrial site (Turkey). Bull. Eng. Geol. Environ. **69**, 397–410 (2010). https://doi.org/10.1007/s10064-010-0290-2
39. Kazemian, S.; Prasad, A.; Huat, B.; Barghchi, M.: A state of art review of peat: geotechnical engineering perspective. Int. J. Phys. Sci. **6**, 1974–1981 (2011)
40. Zainorabidin, A.; Mansor, S.: Investigation on the shear strength characteristic at Malaysian peat. ARPN J. Eng. Appl. Sci. **11**, 1600–1606 (2016)
41. ASTM International.: C150 Cement; Lime; Gypsum. West Conshohocken (2004)
42. Yang, J.: Influence zone for end bearing of piles in sand. J. Geotech. Geoenviron. Eng. **132**, 1229–1237 (2006). https://doi.org/10.1061/(asce)1090-0241(2006)132:9(1229)
43. Hamed, N.; Khairul, A.; Yah, C.: Soil improvement by reinforced stone columns based on experiments works. Electron. J. Environ. Agric. Food Chem. **10**, 2460–2478 (2011)
44. Orekanti, E.; Dommaraju, G.: Load-settlement response of geotextile encased laterally reinforced granular piles in expansive soil under compression. Int. J. Geosynth. Gr. Eng. **5**, 1–8 (2019)
45. Bouassida, M.; Hazzar, L.: Novel tool for optimised design of reinforced soils by columns. In: Proceedings of the Institution of Civil Engineers-Ground Improvement, pp. 31–40 (2012)
46. Brinkgreve, R.B.J.: PLAXIS 3D Tutorial Manual Connect Edition V21 (2021)
47. Brinkgreve, R.B.J.; Kumarswamy, S.; Swolfs, W.M.: PLAXIS 2016 Manual (2016)
48. Salahudeen, A.; Sadeeq, J.: Investigation of shallow foundation soil bearing capacity and settlement characteristics of Minna City Centre development site using Plaxis 2D software and empirical formulations. Niger J. Technol. **36**, 663–670 (2017)
49. Borges, J.; Marques, D.: Geosynthetic-reinforced and jet grout column-supported embankments on soft soils: numerical analysis and parametric study. Comput. Geotech. **38**, 883–896 (2011)
50. Guetif, Z.; Bouassida, M.; Debats, J.M.: Improved soft clay characteristics due to stone column installation. Comput. Geotech. **34**, 104–111 (2007)
51. Algin, H.M.: Optimised design of jet-grouted raft using response surface method. Comput. Geotech. **74**, 56–73 (2016)
52. Algin, H.M.: Optimised design of jet-grouted rafts subjected to nonuniform vertical loading. KSCE J. Civ. Eng. **22**, 494–508 (2018)
53. Zhang, W.; Li, Y.; Goh, A.T.C.; Zhang, R.: Numerical study of the performance of jet grout piles for braced excavations in soft clay. Comput. Geotech. **124**, 103631 (2020)

54. Han, J.; Oztoprak, S.; Parsons, R.L.; Huang, J.: Numerical analysis of foundation columns to support widening of embankments. Comput. Geotech. **34**, 435–448 (2007)
55. Yi, Y.; Liu, S.; Du, Y.; Jing, F.; Gong, N.: Comparison of performance between cross shaped and conventional deep mixed columns for three-layered soft ground improvement under embankment load. In: Ground Improvement and Geosynthetics, pp. 65–70 (2010)
56. Broere, W.; van Tol, A.F.: Modelling the bearing capacity of displacement piles in sand. In: Proceedings of the Institution of Civil Engineers-Geotechnical Engineering, pp. 195–206 (2006)
57. Wehnert, M.; Vermeer, P.: Numerical analyses of load tests on bored piles. In: Proceedings of the 9th International Symposium on Numerical Methods in Geomechanics, pp. 505–511 (2004)
58. Briaud, J.-L.; Jeanjean, P.: Load settlement curve method for spread footings on sand. ASCE **2**, 1774–1804 (1994)
59. Brinch Hansen, J.: Discussion of hyperbolic stress–strain response: cohesive soil. J. Soil Mech. **89**, 241–242 (1963)
60. De Beer, E.E.; Wallays, M.: Franki piles with overexpanded bases. La Tech. Des Trav. **333**, 48 (1972)
61. Lutenegger, A.; Adams, M.: Bearing capacity of footings on compacted sand. Fourth Int. Conf. Case Hist. Geotech. Eng. **36**, 1216–1224 (1998)
62. Architectural Institute of Japan.: Recommendations for Design of Building Foundations, Tokyo (2001)
63. ASTM International: D1633 Standard Test Methods for Compressive Strength of Molded Soil-Cement Cylinders. West Conshohocken, New York (2007)
64. Stoel, A.: Grouting for pile foundation improvement (2001)
65. Wang, Z.F.; Sun, W.J.; Shen, S.L.; Xu, Y.S.; Kim, Y.H.: Quick-gelling of soft soil with jetgrouting using two binders. In: Proceedings of the International Conference on Ground Improvement and Ground Control (2012)
66. AL-Kinani, A.M.; Ahmed, M.D.: Field study of the effect of jet grouting parameters on strength based on tensile and unconfined compressive strength. In: IOP Conference Series: Materials Science and Engineering, p. 012083. IOP Publishing (2020)
67. Guler, E.; Secilen, G.G.: Jet grouting technique and strength properties of jet grout columns. In: Journal of Physics: Conference Series, p. 012006 (2021)